$O_2(^1\Delta)$ production in flowing He/O_2 plasmas. II. Two-dimensional modeling

Ramesh Arakoni[a)]
Department of Aerospace Engineering, University of Illinois, Urbana, Illinois 61801

D. Shane Stafford[b)]
Department of Theoretical and Applied Mechanics, University of Illinois, Urbana, Illinois 61801

Natalia Y. Babaeva[c)] and Mark J. Kushner[d)]
Department of Electrical and Computer Engineering, Iowa State University, Ames, Iowa 50011

(Received 18 May 2005; accepted 23 August 2005; published online 12 October 2005)

In conventional chemical oxygen-iodine lasers (COIL) the 1.315 μm transition in atomic iodine is pumped by a sequence of reactions of I_2 and I with $O_2(^1\Delta)$ which is generated using liquid chemistry. Ongoing studies are investigating means to produce the $O_2(^1\Delta)$ precursor with an electric discharge (eCOIL) to enable a totally gas phase system. Due to the thermodynamic and power loading requirements, the plasma in eCOIL systems is sustained in a flow of a rare-gas diluent and the O_2. In previous investigations, the scaling of production of $O_2(^1\Delta)$ was investigated using global-kinetics and one-dimensional (1D) models. It was found that the production of $O_2(^1\Delta)$ scaled linearly with energy deposition for moderate loadings (a few eV/O_2 molecule). In this paper, these previous investigations are extended to two-dimensions using a plasma hydrodynamics model. The goal of this investigation is to determine if multidimensional considerations affect energy scalings for production of $O_2(^1\Delta)$. We found that $O_2(^1\Delta)$ production generally does scale linearly with energy loading, however, the saturation of $O_2(^1\Delta)$ production occurs at lower-energy loadings than predicted with global and 1D models. This trend is a result of the more accurately depicted and more localized energy deposition afforded by the two-dimensional model, and emphasizes the need for volumetrically uniform power deposition to optimize $O_2(^1\Delta)$ production. © *2005 American Institute of Physics*. [DOI: 10.1063/1.2076428]

I. INTRODUCTION

Chemical laser operation on the $^2P_{1/2} \rightarrow {}^2P_{3/2}$ transition in atomic iodine has been investigated due to its high efficiency and potential for multikilowatt cw power.[1–6] The chemical oxygen-iodine laser (COIL) dissociates I_2 by collisions with metastable $O_2(^1\Delta)$. Subsequent collisions with $O_2(^1\Delta)$ then excite the atomic iodine in a near resonant transfer to create a population inversion and lasing. In order to achieve the flow rates and temperatures required for high-power applications, the gas stream is often expanded through a supersonic nozzle. Conventional COILs generate the $O_2(^1\Delta)$ with yields up to 0.7 using liquid-phase chemistry by reaction of Cl_2 in basic H_2O_2.[7] This method is not optimum for some applications because of the complexity, weight, and operational hazards associated with the liquid chemical storage and pumping systems. Therefore, recent efforts have been investigating the development of all gas phase $O_2(^1\Delta)$ generators based on use of electric discharges (eCOIL). Progress in the production of $O_2(^1\Delta)$ in electric discharges and development of eCOIL lasers are reviewed in Ref. 8 and the companion Paper I (Ref. 9).

In previous works, the scaling of production of $O_2(^1\Delta)$ was computationally investigated using global-kinetics[8] and one-dimensional (1D) models (Paper I). Using the global-kinetics model, we found that yields of $O_2(^1\Delta)$ increase linearly with O_2 specific energy deposition α up to a saturation regime at 5–8 eV/O_2 molecule before decreasing again as O_2 dissociation begins to dominate the kinetics. We also found that the dissociation fraction reaches 0.5 when the peak $O_2(^1\Delta)$ yield occurs, and this reduction in the ground-state density is partly responsible for the saturation in yield. This energy scaling depends on He dilution, power, and pressure, and moderate variations in these parameters produce up to a 50% variation in the peak yield at a given energy deposition, though these variations are weaker when considering the combined yield of $O_2(^1\Delta)$ and $O_2(^1\Sigma)$.

Similar energy scalings for the production of $O_2(^1\Delta)$ yield were obtained with the 1D model described in Paper I that accounts for upstream and downstream expansions of the plasma. In the global model, all power deposition processes are local. In the absence of transport (other than plug flow), power deposition can be optimized while functionally holding all other parameters constant. The improved representation of the transport kinetics of charged and neutral species in the 1D model provide some constraints that do not allow independent optimization of parameters. As a result, the yields predicted by the 1D model are fractionally smaller than those predicted with the global-kinetics model.

In this paper, we extend our computational investigation of energy scaling of $O_2(^1\Delta)$ yields in flowing He/O_2 plasmas using a two-dimensional (2D) model. We found that when considering the full range of flow dynamics, $O_2(^1\Delta)$ production generally does scale linearly with energy loading. The

[a)]Electronic mail: arakoni@uiuc.edu
[b)]Electronic mail: dstaffor@uiuc.edu
[c)]Electronic mail: natalie5@iastate.edu
[d)]Author to whom correspondence should be addressed; electronic mail: mjk@iastate.edu

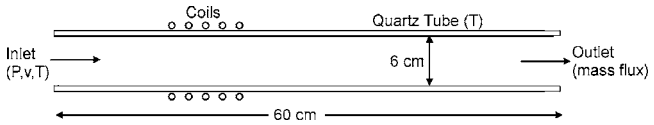

FIG. 1. Schematic of the discharge tube. The flow enters uniformly from the left where pressure, speed, and temperature are specified. The walls are held at constant temperature and mass flux is conserved at the outlet.

saturation of $O_2(^1\Delta)$ production does, however, occur at lower-energy loadings than predicted with the global and 1D models. This trend is a result of the more accurately depicted and more localized energy deposition afforded by the 2D model. These results emphasize the need for making power deposition as uniform as possible to optimize yield. In doing so, the energy loading for any given O_2 molecule or fluid element is made as low as possible, thereby keeping the scaling of $O_2(^1\Delta)$ production as a function of energy deposition in the linear regime. This care also reduces the likelihood that any given O_2 molecule bypasses the plasma and is not excited.

The model and reaction mechanism are briefly described in Sec. II followed by a discussion of $O_2(^1\Delta)$ production in Sec. III. Concluding remarks are in Sec. IV.

II. DESCRIPTION OF THE MODEL

A schematic of the eCOIL device first modeled here appears in Fig. 1. A He/O_2 mixture is flowed through a quartz tube where the plasma is sustained by an inductive discharge. Experimentally, powers of tens to hundreds of watts are deposited into gases flowing at hundreds to thousands of cm/s at pressures of a few to 10 Torr for O_2 mole fractions of up to 50%. The discharge section is usually 10 to a few tens of centimeters in length and many centimeters in diameter. Downstream of the plasma zone, a region not investigated here, the excited gas mixture is fed through a nozzle for supersonic expansion where I_2 is also injected into the flow. The gases then mix, react, and cool as they flow through the transonic and supersonic portions of the nozzle. Ideally the gases are cooled to around 140 K prior to entering the laser cavity and are drawn into the exhaust system.

The model employed in this study is based on nonPDPSIM, which is described in detail in Ref. 10. nonPDPSIM will be briefly described here with emphasis on improvements and modifications made for this study. nonPDPSIM, is a multifluid, 2D hydrodynamics model in which transport equations for all charged and neutral species, and Poisson's equation, are integrated as a function of time. The numerical grid uses a boundary fitting, unstructured mesh with triangular elements. The time evolution of charged particle densities and surface charges are simultaneously solved with Poisson's equation using an implicit Newton's method. This update is then followed, in a time splicing manner, with an implicit update of neutral particle densities and electron temperature. The fluid averaged advective velocity $\vec{v}$ is obtained by solving a modified form of the compressible Navier Stokes equations in which momentum transfer from ion and electron acceleration by the electric field are included in the momentum equation, and Joule heating is included in the energy equations. These equations are solved identically to the method described in Ref. 10. The values of interests are in the steady state which were obtained by a time integration. As such, the time steps used in each successively executed module are not necessarily the same.

In an improvement to the previous 2D model, inductively coupled electromagnetic fields are also addressed by solving the frequency domain form of the wave equation,

$$\nabla^2 E_\theta - \mu_o \varepsilon \frac{\partial^2 E_\theta}{\partial t^2} = \mu_o \sigma \frac{\partial E_\theta}{\partial t} + \mu_o \frac{\partial J_\theta}{\partial t}, \tag{1a}$$

$$\nabla^2 E_o + \mu_o \varepsilon \omega^2 E_o - i\omega\mu_o \sigma E_o = i\mu_o \omega J_o, \tag{1b}$$

where the azimuthal electric field is $E_\theta(\vec{r},t)=E_o(\vec{r})\exp(i\omega t)$ for complex amplitude E_o and radian frequency ω, and the antenna current is $J_\theta(\vec{r},t)=J_o(\vec{r})\exp(i\omega t)$ for complex amplitude J_o. Using finite-volume techniques, Eq. (1b) can be discretized at mesh node i as

$$E_{oi}\left(-\sum_j \frac{A_{ij}}{d_{ij}\Delta V_i} + (\mu_o \varepsilon \omega^2 - i\omega\mu_o\sigma)\right) = -\sum_j \frac{A_{ij}E_{oj}}{d_{ij}\Delta V_i} + i\mu_o \omega J_{oi}, \tag{2}$$

where the sums are over neighboring nodes of i, A_{ij} is the area of the face between the volume cells centered on nodes i and j, d_{ij} is the distance between nodes i and j, and ΔV_i is the volume of the cell for node i. Using successive-over-relaxation (SOR) techniques, E_{oi} is solved by iterating on the expression

$$E_{oi}^{n+1} = E_{oi}^n(1-\alpha) + \alpha\left(\frac{\sum_j \frac{A_{ij}E_{oj}^n}{d_{ij}\Delta V_i} - i\mu_o\omega J_{oi}}{\sum_j \frac{A_{ij}}{d_{ij}\Delta V_i} - (\mu_o\varepsilon\omega^2 - i\omega\mu_o\sigma)}\right), \tag{3}$$

where α is the SOR parameter and the superscript denotes the iteration number.

The boundary conditions were enforced by specifying inlet mole fractions, pressure, temperature, and a flow rate. Since the chemistry is nondepositing (or etching) on bounding materials, the total mass flow through the system must be conserved. The boundary conditions for outlet speeds at the pump port were obtained by requiring such conservation while up-winding values of densities from adjacent grid points in the plasma.

The reaction mechanism for He/O_2 plasma chemistry used here is essentially the same as that described in Ref. 8, and so will be only briefly described. The species in the mechanism include ground-state neutrals O_2, O, O_3, and He; vibrational and electronic states O_2(v), $O_2(a\ ^1\Delta)$, $O_2(b\ ^1\Sigma)$, $O(^1D)$, $O(^1S)$, and $He(^2S)$); and ions O_2^+, O^+, He^+, O_2^-, O^-, and O_3^-. [$O_2(v)$ represents the total vibrational population consisting of the first four vibrational levels of O_2.] The complete gas phase reaction mechanism is shown in Tables I and II of Ref. 8. For the conditions of interest (mole fractions

of >5%–10% O_2) only a small fraction of the power deposition is inelastically dissipated in electron collisions with He.

Electronically excited states of O_2 and O, as well as dissociation of O_2, are dominantly produced by direct electron impact with the ground state,

$$e + O_2 \rightarrow O_2(^1\Delta) + e, \tag{4}$$

$$e + O_2 \rightarrow O(^1D) + O + e, \tag{5}$$

$$e + O_2 \rightarrow O + O + e, \tag{6}$$

$$e + O_2 \rightarrow O_2(^1\Sigma) + e. \tag{7}$$

Production of $O_2(^1\Sigma)$ generally results in generation of $O_2(^1\Delta)$ through rapid quenching reactions with O,

$$O + O_2(^1\Sigma) \rightarrow O + O_2(^1\Delta). \tag{8}$$

As the oxygen is dissociated and the atomic O density increases, production of $O(^1D)$ by direct electron impact on O begins to become important. Large rates of production of $O(^1D)$ lead to generation of $O_2(^1\Sigma)$ by

$$O(^1D) + O_2 \rightarrow O + O_2(^1\Sigma), \tag{9}$$

followed by quenching by O to $O_2(^1\Delta)$. As the $O_2(^1\Delta)$ increases to the many percent level, quenching reactions of $O_2(^1\Delta)$ to form $O_2(^1\Sigma)$ and O_2 and electron-impact dissociation to form O and $O(^1D)$ begin to become important. At this point energy pooling and quenching reactions with $O_2(^1\Delta)$, O_3, and O also begin to reduce $O_2(^1\Delta)$ yields.

The yield of the sum of $[O_2(^1\Delta)]+[O_2(^1\Sigma)]$ will be quoted in terms of a ratio with the mole-fraction equivalent O_2,

$$Y = \frac{[O_2(^1\Delta)] + [O_2(^1\Sigma)]}{[O_2(^3\Sigma)] + [O_2(v)] + [O_2(^1\Delta)] + [O_2(^1\Sigma)] + 0.5[O] + 1.5[O_3]}. \tag{10}$$

This choice of yield was made with the prior knowledge that the majority of $O_2(^1\Sigma)$ is quenched directly to $O_2(^1\Delta)$, and so the most relevant parameter for the best case energy scaling is $[O_2(^1\Delta)]+[O_2(^1\Sigma)]$.

III. SCALING OF THE YIELD OF $[O_2(^1\Delta)]+[O_2(^1\Sigma)]$

A. Inductive coupling

Using the geometry shown in Fig. 1, the base case operating conditions are $He/O_2=70/30$, 3 Torr, flow rate of 6 standard-liters/minute (lpm), inlet gas temperature of 300 K, and power deposition of 40 W ($\alpha=0.3$ eV/O_2). The temperature of the walls was held at 300 K assuming there to be active water cooling. The tube dimensions are a diameter of 6 cm and length of 60 cm. In this section, we discuss results for pure inductively coupled power provided by coils having four turns and length of 10 cm. Capacitive coupling will be discussed in Sec. III B. We use azimuthally symmetric cylindrical coordinates and so all 2D images show only the radial and axial dimensions.

The electric field, power deposition, electron temperature T_e, and electron density are shown in Fig. 2 for the base case. Assuming pure inductive coupling, power deposition is highly peaked off axis with a maximum value of 3.5 W/cm^3. This produces a peak value of T_e of 2.6 eV. The region of elevated T_e extends significantly beyond the peak in power deposition and coils due to the large electron thermal conductivity. The resulting electron density $[e]$ has a highly confined off-axis peak of 2.3×10^{11} cm^{-3}. This confinement results from dissociative attachment to He/O_2 that rapidly consumes electrons in the plasma volumes where T_e =1.5–2 eV. These are values where the rate coefficient for attachment is reasonably large while the rates of ionization are negligible. Power deposition, T_e, and $[e]$ are displaced downstream from the middle of the coils also due to gas flow entraining ions through momentum transfer collisions and shifting them downstream. Ambipolar forces then drag the electrons along.

Thermodynamic properties (gas temperature, mass density, and flow rate) and species [He, O_2, O, $O_2(^1\Delta)$, $O_2(^1\Sigma)$] densities are shown in Fig. 3 for the base case. The gas temperature T_g increases by 53 K above ambient, peaking in the vicinity of the maximum power deposition. Thermal condition and heat transfer at the walls translate the peak in T_g to the axis while the gas cools downstream, first at the walls. The gas returns to near ambient values at the exit. The resulting gas rarefaction closely follows; deal-gas behavior, producing a decrease in mass density of nearly 20%. In order to keep the radially averaged mass flux constant along the axis, the axial speed increases from 1030 at the entrance to about 2000 cm/s on axis where the rarefaction also is maximum. Based on gas heating alone, the increase in speed should be only to 1200 cm/s. The larger increase results from electron-impact dissociation of O_2 that increases the total gas number density. The gas flow must then increase in order to maintain a constant pressure.

The rates of excitation and ionization of the He buffer gas are negligible, and so the spatial distribution of the density of He mimics that of the mass density. These spatial distributions are, however, not identical due to the dissociation of O_2 that occurs in the plasma zone. The increase in total number density and the resulting increase in pressure produces a nonthermally induced increase in speed and gradients in the density of species. He, having the largest diffusivity, responds most quickly to these gradients.

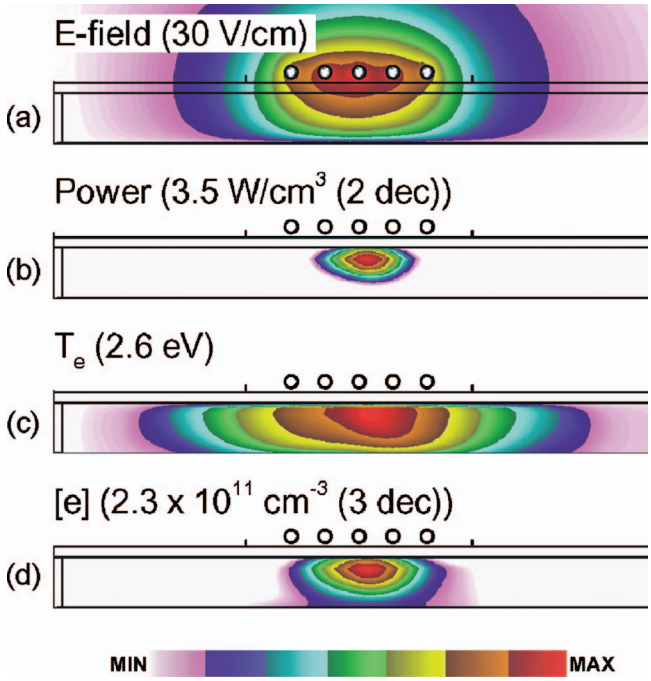

FIG. 2. (Color) Plasma properties for the base case conditions (He/O_2 =70/30, 3 Torr, 6 lpm, 40 W, α=0.3 eV/O_2). (a) Inductively coupled electric field, (b) power deposition, (c) electron temperature, and (d) electron density. The flow is from the left and only the first 30 cm of the tube are shown. The maximum value is indicated in each figure. Scales are linear with zero minimum values unless the number of decades (i.e., "decs") is indicated for log plots. Assuming purely inductive coupling, power deposition is peaked off axis and displaced slightly upstream due to flow effects.

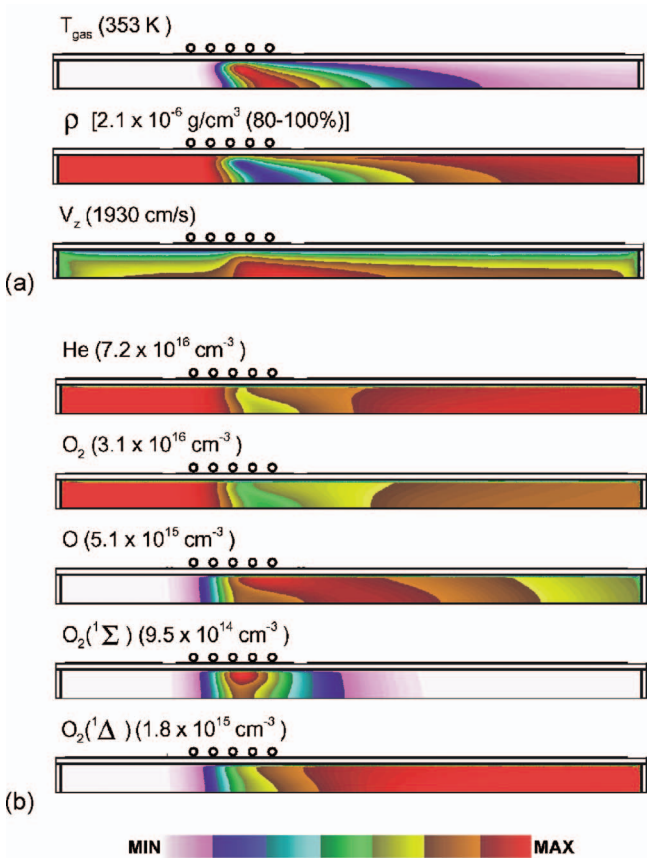

FIG. 3. (Color) Flow properties and species densities for the base case conditions (He/O_2=70/30, 3 Torr, 6 lpm, 40 W, α=0.3 eV/O_2). The flow is from the left. (a) Gas temperature, mass density, and axial speed, and (b) densities of He, O_2, O, $O_2(^1\Sigma)$, and $O_2(^1\Delta)$. The maximum value is indicated in each figure with minimum values being zero with the exception of mass density. Gas heating by the localized power deposition produces peak axial speeds of nearly 20 m/s. $O_2(^1\Delta)$ maximizes downstream in part due to quenching of $O_2(^1\Sigma)$.

Electron-impact processes in the plasma zone, dissociation, and excitation, contribute to depletion of ground-state O_2 in addition to that due to rarefaction. Electron-impact dissociation produces about 10% of the depletion with an additional 10% coming from electron-impact excitation to $O_2(^1\Delta)$ and $O_2(^1\Sigma)$. The density of O atoms peaks 30 cm downstream, decreasing thereafter due to recombination on the walls, and three-body association reactions in the gas phase to form O_2 and O_3.

Direct electron-impact excitation of $O_2(^1\Delta)$ and $O_2(^1\Sigma)$ is only significant in the plasma zone, extending a few centimeters downstream of the coils. The rate coefficient for electron-impact excitation of $O_2(^1\Delta)$ is maximum for $T_e \approx 1$ eV which occurs downstream of the coils and which partly compensates for the decrease in electron density. The density of $O_2(^1\Sigma)$ peaks in the plasma zone where production is largest and is rapidly quenched to $O_2(^1\Delta)$ by collisions with O atoms. The density of $O_2(^1\Delta)$ ceases to increase when the $O_2(^1\Sigma)$ is depleted, and then only moderately decreases due to quenching.

Excited states of O_2 and atomic O also extend 5–10 cm upstream of the plasma zone, commensurate with the predictions from the 1D model. Here, this extension of excited states is dominantly a result of upstream diffusion and secondarily due to local excitation by the plasma that may extend upstream.

The density of $O_2(^1\Delta)$ is shown in Fig. 4(a) for different power depositions but for otherwise the base case conditions (He/O_2=70/30, 3 Torr, 6 lpm). The fractional dissociation and combined yield of $O_2(^1\Delta)$ and $O_2(^1\Sigma)$ on the axis for the same conditions are shown in Fig. 5. The peak dissociation progressively moves downstream as the power increases due in large part to the increasing gas temperature, rarefaction, and extension of the plasma zone. The combined yield is maximum in the plasma zone and experiences an immediate decrease at the edge of the plasma zone where excitation rates have diminished but superelastic quenching is still important. The yield is nearly constant thereafter, only slowly decreasing due to heavy particle quenching.

Over the range of powers investigated (5–120 W, α =0.04–0.9 eV/O_2), the combined yield becomes sublinear with power for values exceeding 70–80 W ($\approx$0.6 eV/O_2), as shown in Fig. 5(c). Results from the global and 1D modelings, imply that the combined yield should scale linearly with α to higher values. We attribute the less favorable scaling found here to non uniform power deposition which is exacerbated by the pure inductive coupling. The nonuniform deposition allows some fraction of the feedstock gas to bypass the region of peak power deposition without being excited. This results in that portion of the flow which does pass through the region of peak power deposition to experience a larger effective value of α to provide the specified flow averaged value of α. Estimates of the effective energy deposi-

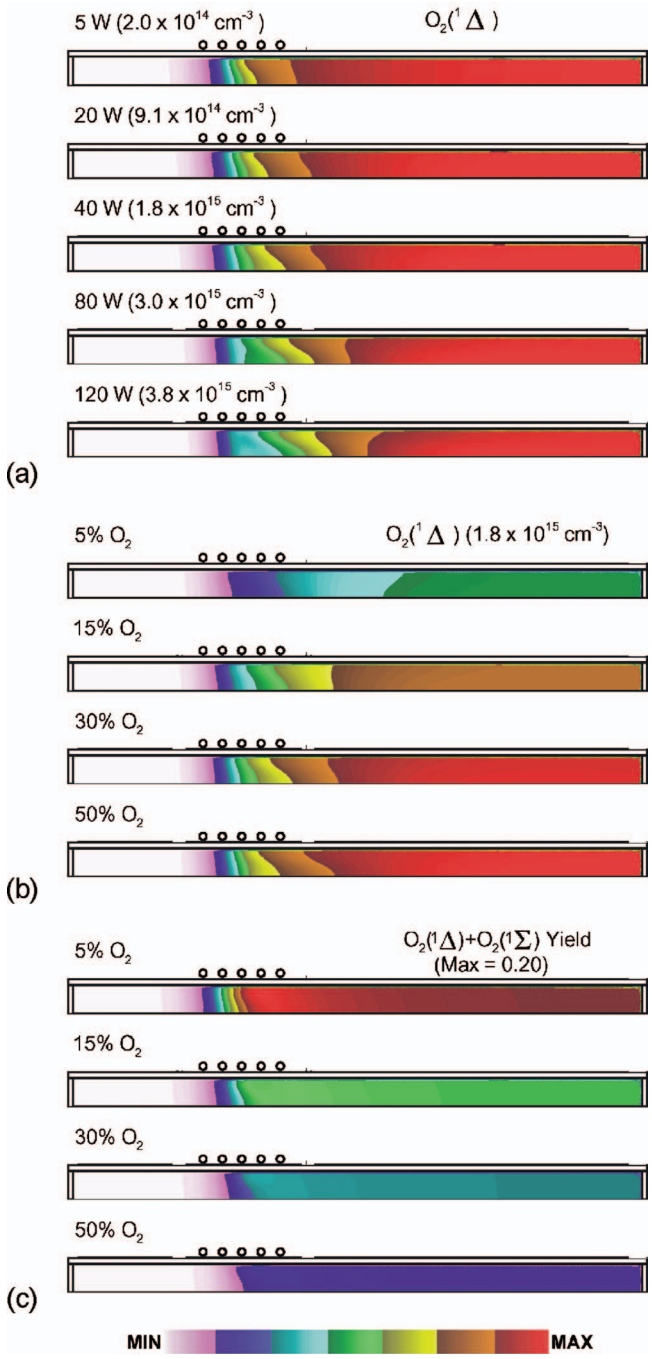

FIG. 4. (Color) Densities of $O_2(^1\Delta)$ and $O_2(^1\Sigma)$ while varying power and O_2 fraction (3 Torr, 40 W). The flow is from the left. (a) $O_2(^1\Delta)$ for O_2 fraction of 30% and powers of 5–120 W (α=0.04–0.9 eV/O_2), (b) $O_2(^1\Delta)$ for a power of 40 W and O_2 fractions of 5%–50%, and (c) combined yield of $O_2(^1\Delta)$ and $O_2(^1\Sigma)$ for 40 W and O_2 fractions of 5%–50% (α =0.18–1.8 eV/O_2). The maximum value is indicated in each figure with minimum values being zero. Although the $O_2(^1\Delta)$ increases downstream, the combined yield reaches its maximum value at the end of the plasma zone.

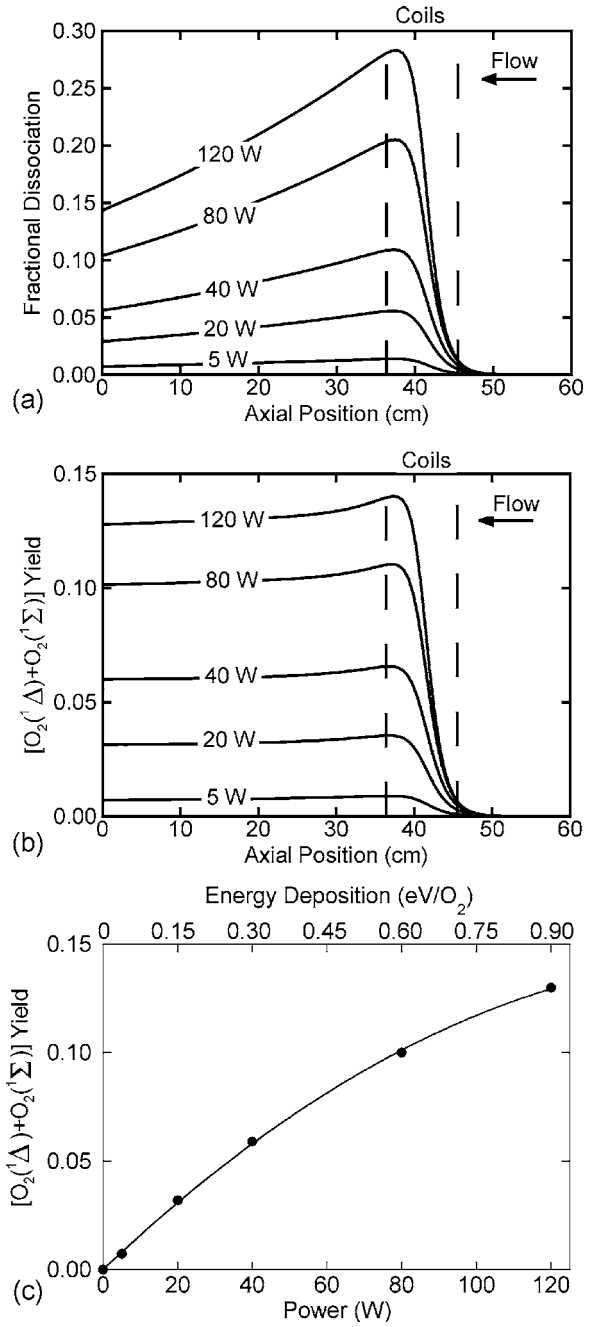

FIG. 5. Plasma properties for different power depositions (He/O_2=70/30, 3 Torr, 6 lpm). (a) Fractional dissociation and (b) combined yield of $O_2(^1\Delta)$ and $O_2(^1\Sigma)$ along the axis. The flow is from the right. (c) Exit yields as a function of power and energy deposition. Maximum yields are established within the range of the coils. Yields begin to saturate early due to nonuniform power deposition.

tion in the plasma zone net values of α=6–8 eV/O_2 are sufficiently large that sublinear scaling of yield should be expected.

The density of $O_2(^1\Delta)$ and the combined yield as a function of position are shown in Figs. 4(b) and 4(c) while varying the O_2 fraction (5%–50%, α=1.8–0.18 eV/O_2) but for otherwise the base case conditions. Fractional dissociation, combined yield, and the sum of the densities of $O_2(^1\Delta)$ and $O_2(^1\Sigma)$ along the axis are shown in Fig. 6. Commensurate with the increase of α as the O_2 fraction decreases, the fractional dissociation approaches 0.5 for an initial O_2 mole fraction of 5%. Based on volume averaged power deposition, the maximum specific energy deposition (α=1.8 eV/O_2 at 5% O_2) is well below the optimum value of α=8 eV/O_2 for maximizing yield predicted by the global model, and so yield should scale linearly with specific energy deposition. The sublinear increase with increasing α (decreasing O_2 fraction) is largely a result of gas bypassing the plasma zone and there

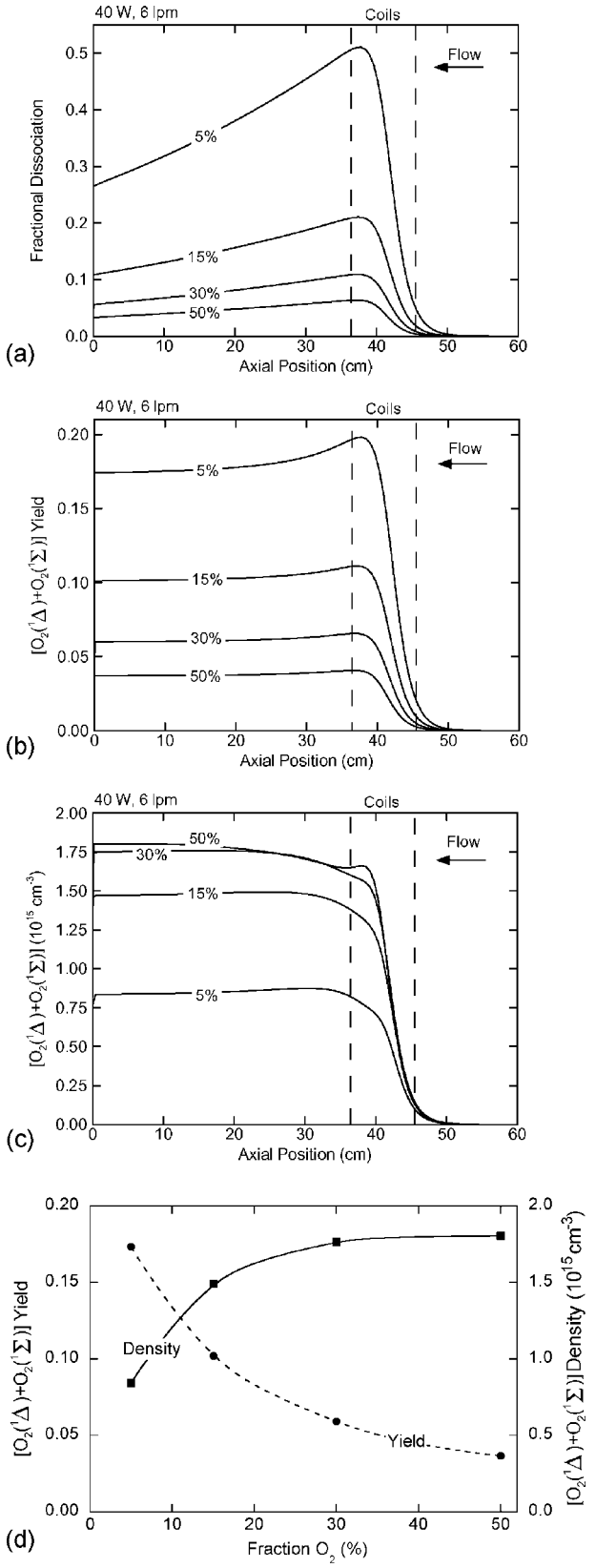

FIG. 6. Plasma properties for different O_2 fractions (40 W, 3 Torr, 6 lpm). (a) Fractional dissociation, (b) combined yield of $O_2(^1\Delta)$ and $O_2(^1\Sigma)$, and (c) combined density of $O_2(^1\Delta)$ and $O_2(^1\Sigma)$ along the axis. The flow is from the right. (d) Exit yield and combined densities as a function of O_2 fractions. Yield and fractional dissociation decrease with increasing O_2 fraction as the $\alpha(\mathrm{eV}/O_2)$ decreases.

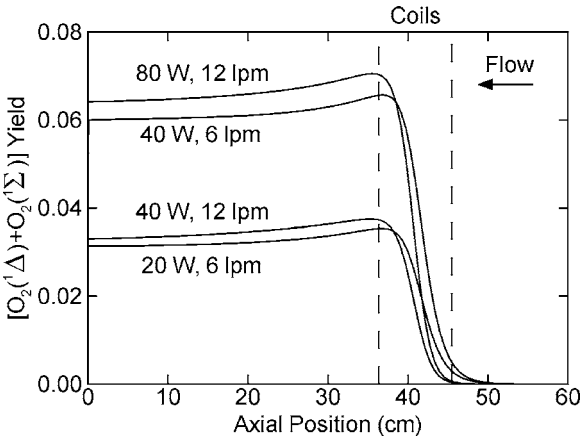

FIG. 7. Combined yield of $O_2(^1\Delta)$ and $O_2(^1\Sigma)$ on the axis of the tube ($He/O_2=70/30$, 3 Torr) for different combinations of flow rates and power deposition that keep $\alpha(\mathrm{eV}/O_2)$ constant. The flow is from the right. For a given value of α the yield is nearly constant, though the production of yield is less efficient at higher-energy loading.

being a larger effective energy deposition for the gas passing through the peak power deposition in the plasma zone.

The efficiency of power utilization in producing excited states while changing the O_2 fraction is indicated by the combined densities of $O_2(^1\Delta)$ and $O_2(^1\Sigma)$ shown in Figs. 6(c) and 6(d). For O_2 fractions exceeding 30%, the fraction of the total power that is channeled into excitation of O_2 is at its maximum value. As a result, increasing the fraction of O_2 to intercept more power yields little additional excitation. The increase in yield obtained when decreasing the fraction of O_2 from 50% simply results from the same density of excited states being produced with a smaller initial mole fraction of O_2. The decrease in the combined excited-state density with lower mole fractions is largely a result of depletion of O_2 and more power being channeled into excitation and ionization of the atomic fragments.

The validity of the energy scaling proposed by the global-kinetics and 1D modeling studies was tested while considering full 2D dynamics. This test was conducted by performing parametrizations where α was held constant while varying flow rates and power deposition. These results are in Fig. 7 where the combined yield on the axis is shown for $He/O_2=70/30$ at 3 Torr. The two cases having power and flow rate of 20 W, and 6 lpm and 40 W and 12 lpm yield $\alpha=0.15$ eV/O_2. The cases having power and flow rate of 40 W and 6 lpm and 80 W and 12 lpm yield $\alpha=0.3$ eV/O_2. For any given pair of conditions yielding the same α, the combined yields are the same within about a relative value of 5%. This level of variation is consistent with the scatter of yields obtained with the global model while varying pressure, flow rate, and power deposition to obtain a given α.

B. Capacitive coupling

A more limited investigation of $O_2(^1\Delta)$ production was performed using capacitive coupling. The geometry is otherwise the same as in the investigation of inductively coupling except that the coils are replaced with two ring electrodes 2 cm wide with centers separated by 13 cm, as shown in Fig. 8(a). The electrodes are powered at 13.56 MHz.

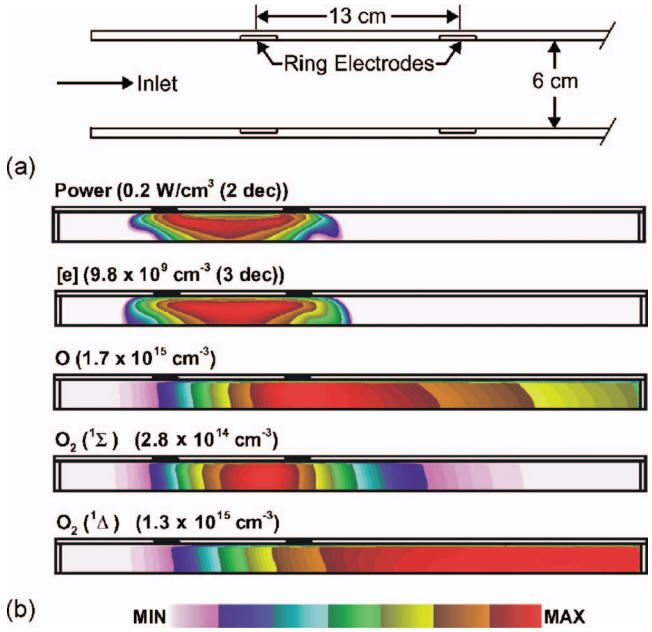

FIG. 8. (Color) Plasma properties for the base case conditions (He/O_2 =70/30, 3 Torr, 6 lpm, 40 W) when using capacitive coupling at 13.56 MHz. (a) Schematic of the electrodes. (b) Power deposition and densities of electrons O, $O_2(^1\Sigma)$, and $O_2(^1\Delta)$. All values are averaged over one rf period. The flow is from the left. Scales are linear with zero minimum values unless the number of decades (i.e., "decs") is indicated for log plots.

Power deposition and densities of electrons, O, $O_2(^1\Sigma)$, and $O_2(^1\Delta)$ are shown in Fig. 8(b) for the base case conditions (He/O_2=70/30, 3 Torr, 6 lpm, 40 W). Values are shown averaged over the rf cycle. With the exception that the power deposition and plasma zone are more extended, there are no significant differences in the characteristics of the capacitively coupled system compared to the pure inductively coupled system. The plasma is more extended in the capacitive system and so the peak electron density and specific power deposition are smaller for the same total power than for the inductively coupled system. Since the production of $O_2(^1\Delta)$ is largely a function of total-energy deposition for these conditions, the lower local power and electron densities resulting from their being more extended in space are not necessarily a detriment. They could, in fact, be beneficial by reducing the likelihood of gas passing around the powered zone.

For these particular conditions, excited-state densities for the capacitively coupled system are 10%–15% smaller than the inductively coupled system. This translates into total yields for capacitive coupling, as shown in Fig. 9 for 5, 20, 40, and 80 W, also being 10%–15% smaller [compare to Fig. 5(b) for inductive coupling]. This lower efficiency is due to power losses to the electrodes, principally ion acceleration and an electron temperature that is a few tenths of an eV higher, on average, than the inductively coupled system. As discussed in Paper I, the efficiency of excitation of $O_2(^1\Delta)$ is optimum for an electron temperature of 1–1.5 eV. The small increase in average electron temperature reduces the efficiency of excitation of $O_2(^1\Delta)$.

IV. CONCLUDING REMARKS

The characteristics of flowing He/O_2 plasmas for the production of $O_2(^1\Delta)$ for use in eCOILs were investigated with a 2D plasma hydrodynamics model. We found that the previously proposed energy scaling stating that the combined yield of $O_2(^1\Delta)$ and $O_2(^1\Sigma)$ is proportional to the energy deposition when expressed as eV/O_2 generally holds. The value of eV/O_2 at which yield increases sublinearly is, however, lower than that predicted by the global kinetics and 1D modelings. This less efficient operation is attributed to flow effects and nonuniform power deposition. The nonuniform power deposition allows for gas to bypass the plasma zone and not be excited. That gas that does pass though the plasma zone experiences a larger effective α to produce the specified flow averaged value of α. As such, $O_2(^1\Delta)$ yield saturates at lower flow averaged values of α. Comparisons between capacitive and inductive coupling showed that there are no significant differences in either plasma characteristics or total yields other than lower peak values of specific power deposition and electron density. The small decreases observed in yields when using capacitive coupling were attributed to electrode losses and a small increase in electron temperature.

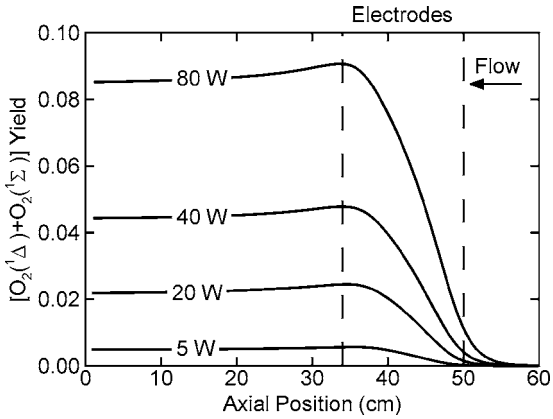

FIG. 9. Combined yield of $O_2(^1\Delta)$ and $O_2(^1\Sigma)$ on the axis of the tube (He/O_2=70/30, 3 Torr, 6 lpm) with capacitive coupling for different powers. Yields are 10%–15% lower than for pure inductively coupling.

ACKNOWLEDGMENTS

This work was supported by the Air Force Research Labs, the Air Force Office of Scientific Research, and the National Science Foundation (CTS 03-15353). The authors thank W. Solomon, J. Zimmerman, D. Carroll, and J. Verdeyen of CU-Aerospace, and T. Madden and G. Hager of the Air Force Research Lab for their insights into the operation of eCOILs.

[1]W. E. McDermott, N. R. Pchelkin, D. J. Benard, and R. R. Bousek, Appl. Phys. Lett. **32**, 469 (1978).
[2]H. Fujii, S. Yoshida, M. Iizuka, and T. Atsuta, J. Appl. Phys. **67**, 3948 (1990).
[3]A. Elior, B. D. Barmashenko, E. Lebiush, and S. Rosenwaks, Appl. Phys. B: Lasers Opt. **B61**, 37 (1995).
[4]M. Endo *et al.* IEEE J. Quantum Electron. **34**, 393 (1998).
[5]D. Furman, E. Bruins, V. Rybalkin, B. D. Barmashenko, and S. Rosenwaks, IEEE J. Quantum Electron. **37**, 174 (2001).
[6]J. Kodymova, O. Spalek, V. Jirasek, M. Censky, and G. D. Hager, Appl. Phys. A **77**, 331 (2003).
[7]J. Kodymova and O. Spalek, Jpn. J. Appl. Phys., Part 1 **37**, 117 (1998).
[8]D. S. Stafford and M. J. Kushner, J. Appl. Phys. **96**, 2451 (2004).
[9]D. S. Stafford and M. J. Kushner, J. Appl. Phys. **98**, 073303 (2005).
[10]M. J. Kushner, J. Phys. D **38**, 1633 (2005).